

**NOAO LSST  
OPTICAL DESIGN STUDY  
FINAL REPORT**

This report summarizes the work performed by Photon Engineering, LLC under contract to NOAO in support of the Large Synoptic Survey Telescope (LSST). Two design trades were requested, each requiring an approximately equal amount of time. Design Trade 1 was to evaluate telescope design options with a design provided to NOAO from Lynn Seppela (Lawrence Livermore National Laboratory, LLNL) as a starting point. Design Trade 2 was to perform a sensitivity analysis to begin to assess stability requirements for the operational assembly.

**Statement of Work**

Two design trades have been solicited: throughput vs. image quality and image quality vs. focus technique. The scope of the trade space is limited to perturbations of the existing concepts, so that the basic design form is unchanged. That is, any viable design solution will be a 3-mirror system with a minimum of 3 refractive elements (2 windows/correctors and a filter) to support the proposed ‘dewar in a dewar’ instrument ensemble. The key factors used to assess any potential design are: throughput, image quality, and tolerance sensitivity.

***Tasks***

1. Preliminary telescope design.
  - a. Evaluate system characteristics to determine key design drivers. The goal of this task is primarily to identify the key constraints affecting image quality and throughput. Initial concepts will omit the refractive components to better determine which design form(s) best satisfy the system constraints and goals. Both re-imaging and non-re-imaging design forms may be considered. The advantage of a re-imaging system is that it typically has better stray light rejection characteristics. The current design forms are both non-re-imaging. All design options will otherwise satisfy the system constraints described in Goals – Item 2 below.
  - b. Add refractive elements and re-optimize candidate systems. No more than 4 refractive elements (3 lenses and a filter) are allowed.
  - c. A brief report summarizing the performance (throughput and image quality) of candidate systems will be submitted to NOAO for review. At NOAO’s discretion, the system or systems offering the best combination of throughput and image quality will be further refined and analyzed.
2. Preliminary baffle design. Add baffles to block direct specular illumination of the target area from sources outside the working field of view. In this case, direct specular illumination refers to any ray path that reaches the focal plane without undergoing a scatter event. These paths are most easily identified by ray tracing from the detector outwards. This task does not include a detailed stray light analysis or

- ghost analysis. All optical surfaces are assumed to be pristine and perfect transmitters or reflectors. All non-optical surfaces will be assumed to be perfect absorbers.
3. Evaluate system performance. This task is primarily a refinement of the calculation performed in Task 1c above and will include the effects of baffles and (optionally) performance predictions for five spectral bands.
  4. Evaluate focus mechanisms.
    - a. Evaluate through-focus sensitivity for each of the following 3 options
      - i. instrument ensemble
      - ii. secondary mirror
      - iii. tertiary mirror
    - b. Preliminary sensitivity (tolerance) analysis. Calculate tolerance sensitivity of candidate systems using the best focus compensation identified in Task 4a above. Note that this task does not include a detailed tolerance study; rather it is intended only for use as a preliminary assessment of fabrication risk.
  5. Final report. Submit a report containing the results and conclusions drawn from this study.

## Task 1 – Optical Design Study

### Introduction

Roger Angel et al. originally proposed for NOAO a three-mirror LSST telescope configuration in 2002. It is a centrally obscured, wide field 8.4m aperture telescope operating at  $f/1.25$ . The proposed instrument imaging assembly is a ‘dewar in a dewar’ concept consisting of two refractive correctors, a group of interchangeable spectral filters, and a large-scale array of CCD detectors. The instrument assembly is mounted in the shadow of the secondary mirror obscuration, in the space proximate to the hole in the primary. Best imagery is obtained on a convex curved focal plane having a radius of curvature of 10.7m. The original LSST concept was subsequently modified by Lynn Seppela (LLNL) to flatten the field and improve image quality. Although successful in these regards, the new LSST concept saw a 10% reduction in throughput compared to the Angel design, which significantly affects the science capability of the LSST instrument. Additionally, the new LSST concept requires complex motion of both the tertiary and secondary mirrors to set and maintain focus. In light of these results, NOAO has solicited further design studies to investigate the trade-off between image quality and throughput and to investigate alternative focus compensation techniques.

### Goals

The aim at the conclusion of this work is to have a reference optical design for the 8.4m LSST that can serve as the basis for detailed studies in mechanical design, tolerancing, enclosure design and development of an instrument concept for the purpose of writing a

fully cost estimated funding proposal for the LSST project. The following items are to serve as guidelines for the proposed work:

1. Baseline design: Angel et al. 2000.
2. System requirements and specifications
  - a. Aperture to be 8.4m (effective aperture of no less than 7m)
  - b. Spectral band is 400 nm to 1000 nm, uniformly weighted
  - c. Full circular field of view (FOV) is 3 degrees.
  - d. Plate scale to remain at  $51\mu\text{m} / \text{arcsecond}$ , equates to system  $f/1.25$  for 8.4m aperture.
  - e. Primary mirror f-ratio to fall between  $f/1$  and  $f/1.2$  to fall with reasonable tolerance and fabrication limits.
  - f. Minimum clearance between the ray bundle and the instrument assembly is 25 mm on a radius. The maximum diameter of the instrument assembly is determined by the diameter of the first refractive element.
  - g. Relax the requirement that the final focal surface must be flat. While this is desirable it is not viewed as an absolute requirement to fabricate the focal surface detector array. It is required that any curvature in the final focal surface be kept greater than  $R=20\text{m}$ .
  - h. Image quality is to be assessed by calculating the polychromatic diffraction encircled energy at 5 points over the semi-field of view. The spot diameter used for the encircled energy calculation is 0.2 arcseconds, which corresponds to  $10\mu\text{m}$  at the focal plane. The goal is to achieve encircled energy fractions in excess of 80% across the field of view. Note that this calculation includes diffraction effects resulting from both vignetting and a central obscuration, but does not implicitly include the loss in throughput introduced by these mechanisms.
  - i. Throughput is to be evaluated solely as the collection area lost to obscuration and vignetting. Perfect transmission and reflectivity is assumed for the lenses and mirrors, respectively.
  - j. Evaluate baffled design for each concept so that each can be evaluated with regard to efficiency/throughput on equal grounds.
  - k. Target throughput to meet or exceed original Angel design.
  - l. Center to edge throughput variation to be no worse than Angel et al, preferably better (less variation), but not at the cost of imaging performance.
  - m. The final design should be such that a shutter with the instrument ensemble can be accommodated.
3. Constraint modifications:
  - a. Allow 3rd refractive element for increased degrees of freedom for balancing chromatic aberration and focal surface flatness.
  - b. Relax asphericity constraints on secondary for more flexibility in optimizing design goals. Given plausible testing methodology low asphericity in the secondary is not viewed as a critical design goal.
  - c. Filter substrate to be curved to allow for filter to be telecentric with respect to incoming beam.

- d. Explore instrument (three refractive elements + filter) location to optimize opto-mechanical solutions for support without sacrificing optical performance (image quality and throughput).
- e. Increase distance between focal surface+filter and intermediate refractive element to allow for mechanical movement of filter exchange (minimum of +50mm). This constraint applies primarily to the Seppela design, referred to as the Case4b configuration.
- f. Focus optical system by moving only the instrument ensemble and evaluate performance.

### Task 1a – Parametric Analysis

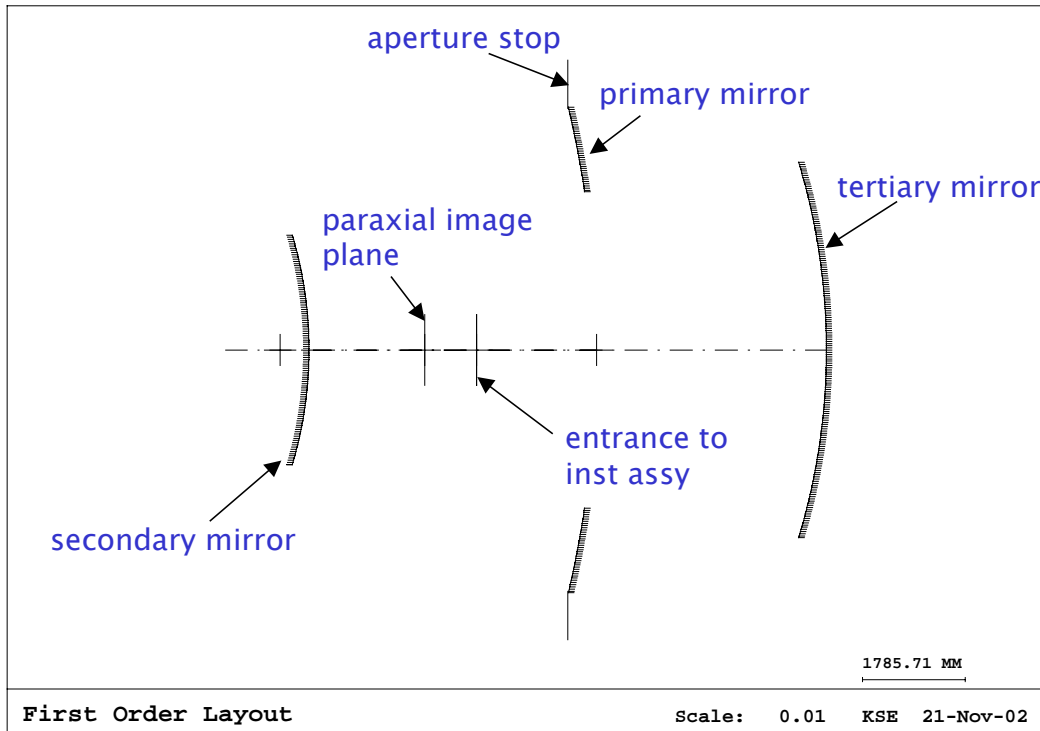


**Figure 1** Basic telescope configuration for parametric analysis of image quality and throughput

A parametric analysis was undertaken to determine if there is a correlation between image quality and throughput, and, if so, what aspects of the telescope design affect the relationship. For this study, only flat-field (i.e., zero Petzval curvature) three mirror configurations were considered. The methodology used for the analysis is as follows:

- Set the primary mirror  $f/\#$
- Set the length of the instrument ensemble. This value is used to establish the location and diameter of the front and back surfaces of the ensemble prior to

calculating throughput. Dummy optical surfaces coincident with the front and back surfaces are used in the model to simulate the resulting obscuration of the instrument assembly.

- Iterate the separation between the mirrors. Separations are fixed prior to optimization. For each iteration the following steps are performed:
  - A curvature solve on the tertiary mirror changes its base radius of curvature so that the system focal length is maintained ( $f = 10.5$  m)
  - The curvature of the secondary mirror is varied during optimization so that the Petzval sum of the telescope equals zero.
  - A paraxial image solve locates the image plane. The separation between the tertiary mirror and the instrument assembly is variable.
  - Optimize. The conic constant and even-order polynomial aspheric coefficients of each mirror are allowed to vary during optimization to improve image quality across the field of view.
  - Subsequent to optimization, the front and back surfaces of the instrument assembly are sized and located, apertures and obscurations are set, and the telescope is evaluated for image quality and throughput. Image quality is assessed as the average RMS wavefront error across the field of view and over the entire spectral band from 0.4 microns to 1.0 microns. Throughput is calculated for an unvignetted system, so it is constant across the field of view. This is somewhat limiting because if vignetting is allowed, better throughput can be achieved for small field angles, but there will be some variation across the field of view. However, because telescope operational parameters will be set based on the worst-case throughput condition, the decision was made at the outset to prohibit vignetting and thereby remove throughput variation across the field of view. For reference, using these assumptions the Case4b telescope design by Lynn Seppela has a maximum fractional throughput of 0.64 and 1.1 waves of RMS error at 0.5 microns.
- Tabulate and print results

Figure 2 shows a compilation of the results. The primary mirror  $f/\#$  was varied between  $f/1.0$  and  $f/1.2$ . The separation between the secondary mirror and the primary mirror was varied between 4000 mm and 6000 mm. The separation between the primary mirror and the tertiary mirror was varied between 3000 mm and 5000 mm. Each data point on the chart represents a specific and unique configuration. Note that in order to meet the minimum throughput requirement which yields an effective 7 m collection aperture, the fractional throughput must be greater than 0.7. RMS wavefront error is averaged across both the field of view and over the entire spectral band from 0.4 microns to 1.0 microns. Reported units are in waves at 0.5 microns.

While it is difficult to establish an exact relationship between image quality and throughput, a few qualitative observations can be made. When the RMS wavefront error is small, both the fractional throughput and the RMS error increase together. As the RMS error continues to increase the fractional throughput goes through a maximum and then

slowly begins to drop again. A faster primary generally yields a higher maximum throughput, but will be harder to correct.

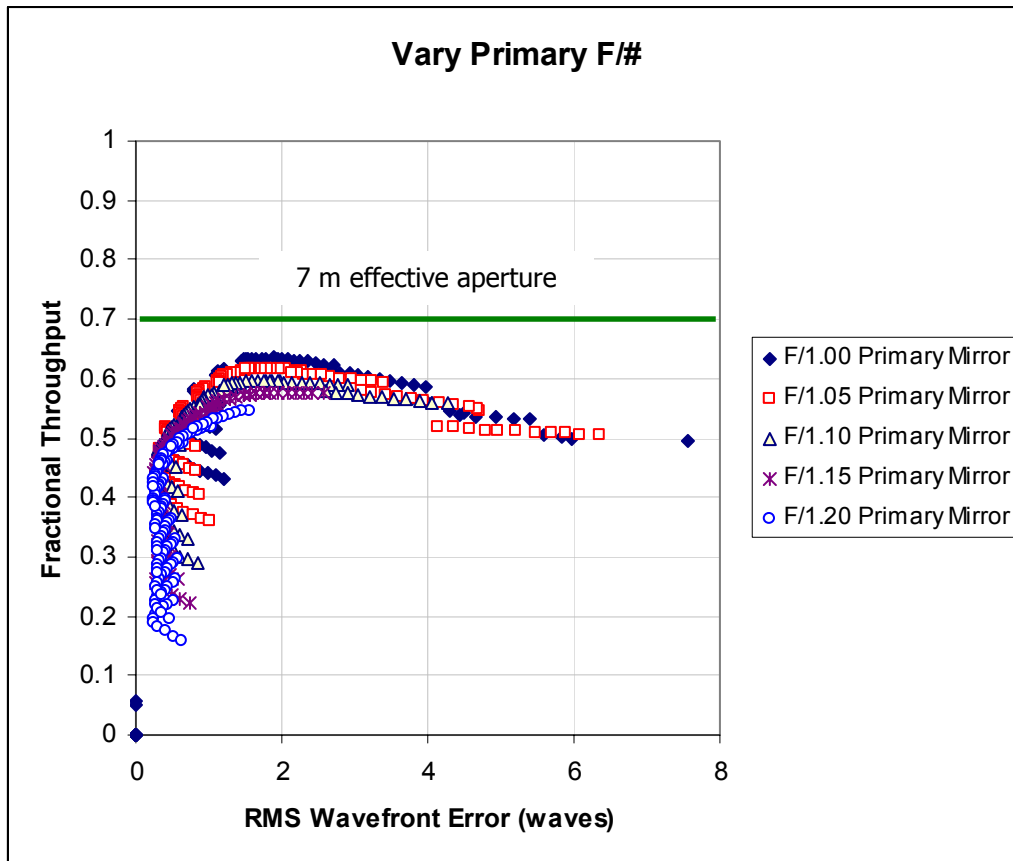
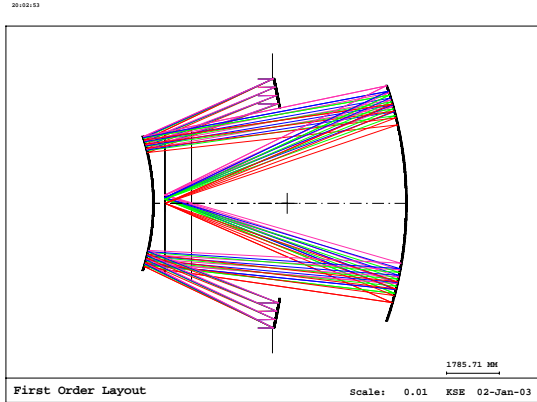


**Figure 2** Correlation between RMS wavefront error and fractional throughput for different primary mirror  $f/\#$ 's. Each data point is a different configuration. Within each data range, the mirror separations are being varied parametrically.

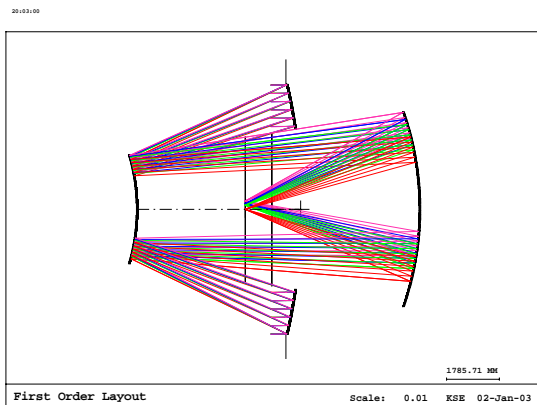
### *Vary Primary/Secondary Mirror Separation*

Varying the separation between the primary and secondary mirrors has a larger effect on both throughput and image quality than does varying the separation between the primary and tertiary mirrors (Figures 3 and 4). There are two main effects at work: the size of the beam footprint on the secondary mirror and its magnification. The first has the effect of increasing the size of the hole in the primary mirror by simple virtue of its physical extent. Even a small amount of divergence requires a large hole in the primary, thereby reducing throughput, even though image quality remains quite good. This is the case for the secondary mirror being close to the primary. The second effect, secondary mirror magnification, increases with mirror separation. As a result, even though the physical extent of the beam at the secondary mirror is small, the divergence of the reflected beam grows. This, coupled with the larger separation, also results in a big hole in the primary

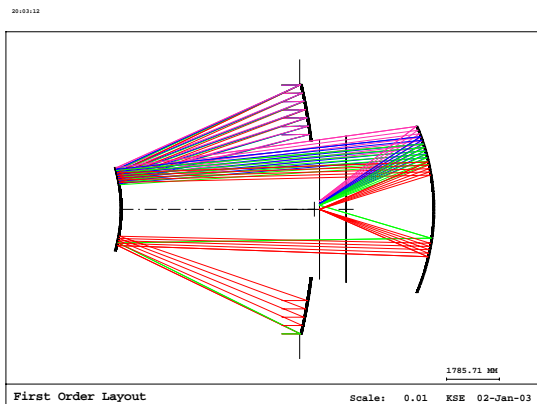
mirror. This is the case in the bottom picture shown in Figure 3. The best performance is achieved when the separation between the primary and secondary mirrors is approximately equal to half of the focal length of the primary mirror.



P/S = 4500 mm  
Throughput = .42  
RMS = .32 waves



P/S = 5500 mm  
Throughput = .59  
RMS = 1.23 waves

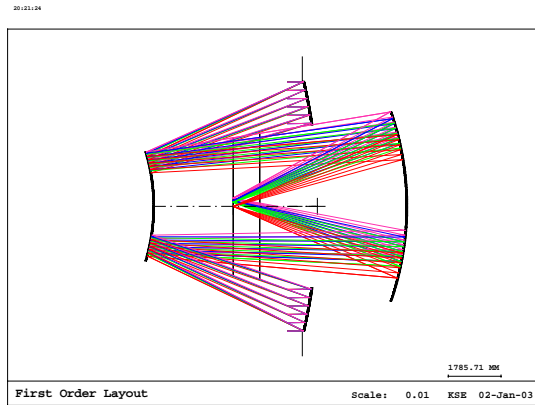


P/S = 6500 mm  
Throughput = .47  
RMS = 8.44 waves

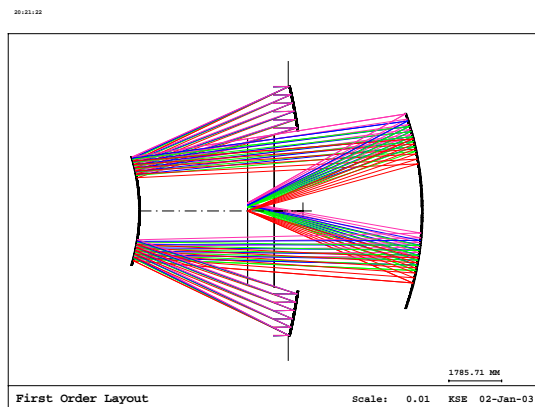
**Figure 3** Varying primary/secondary mirror separation. Primary mirror  $f/\#$  is 1.1 and the separation between the primary and tertiary mirrors is 4000 mm.

### Vary Primary/Tertiary Mirror Separation

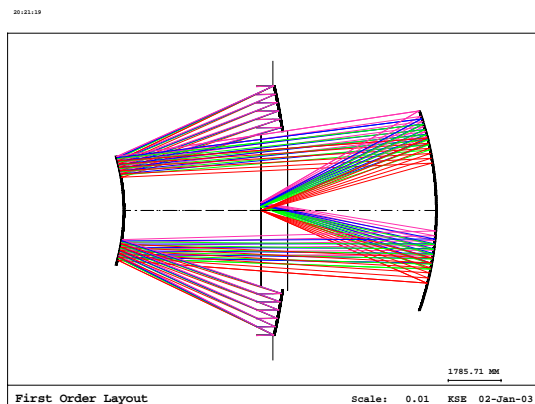
Varying the separation between the primary and tertiary mirrors does not significantly affect system performance (Figure 4).



P/T = 3000 mm  
Throughput = .572  
RMS = 1.02 waves



P/T = 4000 mm  
Throughput = .587  
RMS = 1.23 waves



P/T = 5000 mm  
Throughput = .594  
RMS = 1.62 waves

**Figure 4** Varying primary and tertiary mirror separation. The primary mirror  $f/\#$  is 1.1 and the separation between the primary and secondary mirrors is 5500 mm.

## Task 1b - Design Optimization

The design process began using configurations obtained during the parametric analysis as a starting point. The goal early on was to obtain the best telescope that operated over the entire spectral band from 0.4 microns to 1.0 microns without the use of moving elements. It has already been demonstrated with the Case4b design that exceptionally good imagery can be obtained if the telescope configuration is allowed to change for each of 5 spectral bands (Table 1). The Case4b design has two mirrors moving independently and uses 5 spectral filters, each having a different center thickness. The question is how much performance is sacrificed in the interest of reducing system complexity? Secondary issues also addressed during optimization included increasing the edge thickness of the first (outermost) lens, increasing the center thickness of the second lens, and increasing the clearance between the optical filter and the second lens element to allow for a filter swapping mechanism.

The basic design form is substantially the same as that used in the Case4b design (Figures 5 and 6). There were no specific constraints regarding the surface figure for the mirrors. Likewise for the location and size of the instrument assembly. Each mirror is an even-powered radial asphere with a variable conic constant. The secondary mirror may require polynomial terms up to 10<sup>th</sup> order, while terms up to 6<sup>th</sup> and 8<sup>th</sup> order were generally sufficient for the primary and tertiary mirrors, respectively. The lens elements are fused silica. For lens elements 1 and 2, the convex (front) surfaces are simple spheres and the concave surfaces are aspheric surfaces with even-powered polynomial terms up to 6<sup>th</sup> order and variable conic constants. The filter is a simple plano-plano element. The field-flattening lens is a simple plano-convex element, with the plano surface nearest the detector array. The image surface is assumed flat (no significant benefit was derived by allowing it to curve slightly).

Holes, obscurations, and apertures have been assigned so that all fields pass through the telescope unvignetted. As mentioned earlier, this constraint has the effect of reducing the throughput on-axis but minimizes its variability over the field of view. Image quality is assessed primarily as the amount of energy contained in a 10 micron diameter circle relative to that incident on the image plane. The encircled energy calculation is diffraction based. It takes into account the diffraction effects of holes and obscurations, but ignores the resulting loss in throughput. Additionally, the blur diameters containing 50% and 80% of the energy in the diffraction spot are also calculated, as this metric may be more useful for full-up system performance predictions.

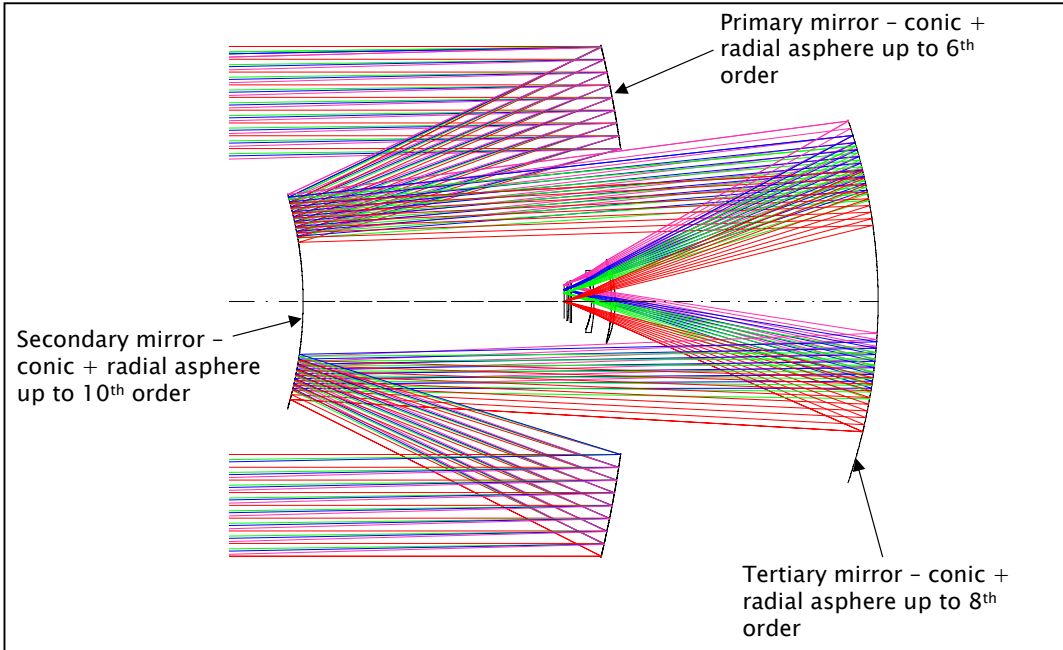


**Figure 6** Basic telescope configuration

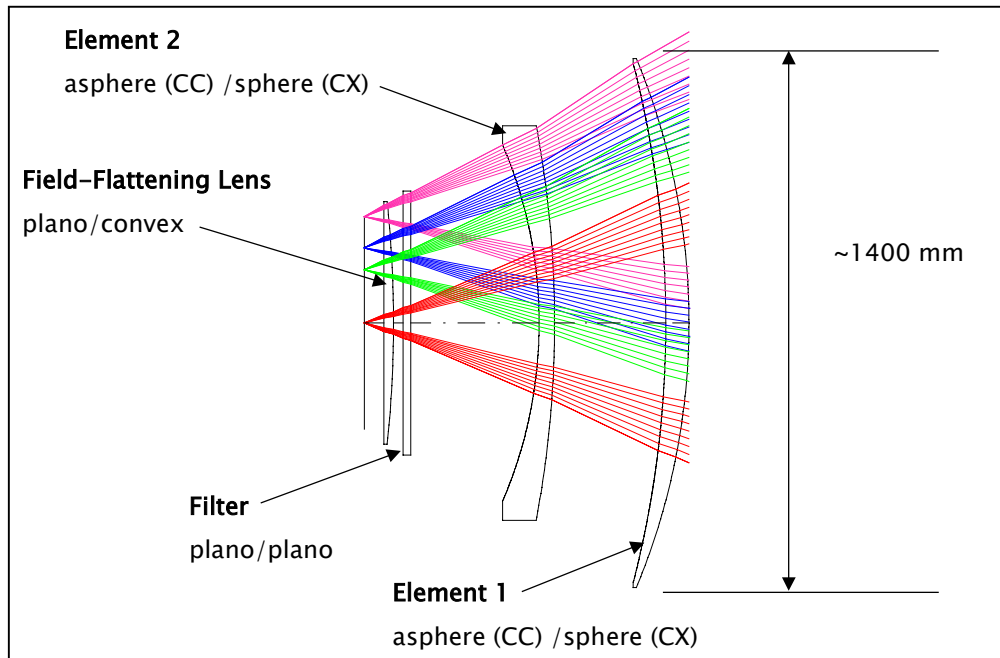


**Figure 5** Instrument assembly detail. A minimum radial clearance of 25 mm is maintained between the outer diameter of Element 1 and the reflected beam.

## Task 1c – Design Summary/Lessons Learned

The telescope configuration shown in Figures 4 and 5 is typical of the solutions obtained during design optimization. As was seen in the parametric analysis, many variants yield comparable performance, both in terms of image quality and throughput. Adding the instrument ensemble does not change this basic result. Variations between good configurations could be quite substantial in terms of the overall system geometry, but a great many solutions had very nearly identical performance. None, however, demonstrates better image quality than that obtained with the Case4b configurations, which moved two mirrors and changed the thickness of the optical filter according to spectral band. This is an important result. A broadband solution does not maintain the same image quality as one in which 2 or more elements are allowed to move. Performance data illustrating this point is shown in Figures 7 and 8. The latter is for a telescope derived from the parametric analysis that has better throughput uniformity across the field of view, does not meet image quality requirements across all bands.

As defined in this analysis, throughput is fundamentally a first-order property of the telescope. Faster primary mirrors generally yield higher fractional throughput, but do so at the expense of image quality. Once a design has begun to converge to a solution, it is extremely difficult to modify. Mirror separations tend not to change, to the extent that in most cases, these separations can be frozen without adversely affecting image quality. The hole in the primary mirror is by far the dominant throughput loss mechanism. Because of this, the size of the instrument assembly is not critical, which allows some flexibility in specifying its overall length. A more practical reason to limit the length of the instrument assembly is to keep the diameter of the first lens element from becoming overly large.

The corrector elements need to be as thin as modern fabrication techniques will allow. The first lens, Element 1, tends to a small edge thickness. In setting up the merit function, it is necessary to maintain strict control of this dimension because the lens design program wants to make it very thin to control chromatic aberration, or, more precisely, the chromatic variation of higher order aberrations. Small changes in the edge thickness of the first element have a large effect on image quality. Element 2 tends towards small center thickness and increasing thickness towards the edge. Increasing the center thickness of Element 2 results in degraded image quality, but the effect is not as significant as increases in the edge thickness of Element 1.

The reason that a single broadband configuration does not perform as well as the Case4b design is the chromatic variation of spherical and coma, particularly at short wavelengths, which manifests itself on a ray intercept plot as a steep flare at one side of the pupil near the edge of the field of view (Figures 9 and 10). The difficulty with correcting these aberrations is multifold. Part of the problem is that the corrector elements are nearly afocal. This is beneficial for reducing axial chromatic aberration, but there is little leverage to be gained from changing the distribution of power between the positive and negative elements. For the same reason, varying the glasses also does not provide much benefit. For example, an equivalent solution can be obtained using all Schott U-BK7

elements in place of fused silica, but mixing glasses did not prove to be an effective means of aberration control. Inserting an additional corrector element or splitting the single elements into doublets also failed to provide improvement over the best fused silica designs. Since the aberrations are chromatic, increasing the number of aspheric terms on the corrector elements also does not improve image quality.

Given all of the apparent limitations of a broadband design, it does have some advantages. Foremost is that, with the exception of the filter swap, all of the optical elements are stationary, thereby reducing system complexity. Additionally, the effective focal length (EFL) of the telescope is virtually unchanged across all five wavelength bands. This is important because the EFL affects the plate scale, so it is desirable to have a constant value across all bands. The EFL of a typical broadband design changes by less than 1 mm moving from the near-IR bands to the near-UV bands. In contrast, the EFL of the Case4b lens changes by 8 mm over the same range. In both cases, the EFL is smaller at the shorter wavelengths.

**Table 1** Table of spectral bands and zoom positions

<b>Band</b>	<b>Spectral Range (nm)</b>	<b>Zoom Position</b>
Z	940 +/- 100	1
I	807.5 +/- 75	2
R	644 +/- 75.5	3
V	537 +/- 47	4
B	436 +/- 49.5	5

```

Case4b Design
80% Encircled energy target diameter (microns): 10.00 (0.2 arc-sec)
+++++
Zoom position 1
Spectral bandpass center wavelength: 940.00 nm
Average RMS wavefront error (waves @ 915.50 nm): 0.131
Relative Field      Throughput(%)      Encircled_Energy(%)      Spot50(um)      Spot80(um)
0.000              70.01             87.53                    3.538           7.076
0.350              68.21             86.73                    3.950           7.739
0.500              67.31             86.27                    4.191           8.097
0.707              66.22             85.99                    4.344           8.396
0.850              64.60             83.28                    4.543           9.193
1.000              61.89             74.20                    5.411           12.122
+++++
Zoom position 2
Spectral bandpass center wavelength: 807.50 nm
Average RMS wavefront error (waves @ 791.40 nm): 0.130
Relative Field      Throughput(%)      Encircled_Energy(%)      Spot50(um)      Spot80(um)
0.000              70.01             88.22                    5.411           12.122
0.350              68.21             88.37                    2.983           6.039
0.500              67.31             88.61                    3.227           6.492
0.707              66.22             88.81                    3.455           6.897
0.850              64.60             86.61                    3.749           7.162
1.000              61.89             79.44                    3.987           7.798
+++++
Zoom position 3
Spectral bandpass center wavelength: 644.00 nm
Average RMS wavefront error (waves @ 624.00 nm): 0.193
Relative Field      Throughput(%)      Encircled_Energy(%)      Spot50(um)      Spot80(um)
0.000              70.01             90.91                    3.987           7.798
0.350              68.21             89.87                    4.594           10.343
0.500              67.31             89.41                    2.417           5.388
0.707              66.22             88.40                    2.614           5.554
0.850              64.60             85.32                    2.998           6.354
1.000              61.89             78.21                    3.738           7.318
+++++
Zoom position 4
Spectral bandpass center wavelength: 537.00 nm
Average RMS wavefront error (waves @ 527.50 nm): 0.224
Relative Field      Throughput(%)      Encircled_Energy(%)      Spot50(um)      Spot80(um)
0.000              70.01             92.28                    3.738           7.318
0.350              68.21             92.54                    4.247           8.420
0.500              67.31             91.89                    4.966           10.505
0.707              66.22             90.75                    2.441           4.949
0.850              64.60             88.42                    2.178           4.691
1.000              61.89             81.99                    2.495           5.147
+++++
Zoom position 5
Spectral bandpass center wavelength: 436.00 nm
Average RMS wavefront error (waves @ 423.10 nm): 0.451
Relative Field      Throughput(%)      Encircled_Energy(%)      Spot50(um)      Spot80(um)
0.000              70.01             87.91                    2.495           5.147
0.350              68.21             90.39                    3.376           6.280
0.500              67.31             89.75                    4.051           7.441
0.707              66.22             87.05                    4.794           9.518
0.850              64.60             82.82                    4.112           7.505
1.000              61.89             73.79                    3.062           7.065

```

Figure 7 Performance predictions of the Case4b design (Seppela) over the 5 spectral bands.

```

Highest Throughput
80% Encircled energy target diameter (microns): 10.00 (0.2 arc-sec)
+++++
Zoom position 1
Spectral bandpass center wavelength: 940.00 nm
Average RMS wavefront error (waves @ 915.50 nm): 0.327
Relative Field Throughput(%) Encircled_Energy(%) Spot50(um) Spot80(um)
0.000 65.68 74.34 6.731 11.198
0.350 65.68 60.53 8.477 13.611
0.500 65.68 54.05 9.426 14.704
0.707 65.50 52.91 9.672 14.953
0.850 65.14 54.48 9.438 16.045
1.000 64.24 47.31 10.875 22.200
+++++
Zoom position 2
Spectral bandpass center wavelength: 807.50 nm
Average RMS wavefront error (waves @ 791.40 nm): 0.303
Relative Field Throughput(%) Encircled_Energy(%) Spot50(um) Spot80(um)
0.000 65.68 86.78 10.875 22.200
0.350 65.68 78.56 4.078 8.050
0.500 65.68 72.29 6.032 10.300
0.707 65.50 71.17 6.944 11.453
0.850 65.14 70.89 7.220 11.621
1.000 64.24 52.17 7.062 12.379
+++++
Zoom position 3
Spectral bandpass center wavelength: 644.00 nm
Average RMS wavefront error (waves @ 624.00 nm): 0.282
Relative Field Throughput(%) Encircled_Energy(%) Spot50(um) Spot80(um)
0.000 65.68 91.29 7.062 12.379
0.350 65.68 90.74 9.395 17.962
0.500 65.68 89.54 2.677 5.245
0.707 65.50 88.71 2.954 6.046
0.850 65.14 85.75 3.635 7.033
1.000 64.24 68.90 4.446 7.436
+++++
Zoom position 4
Spectral bandpass center wavelength: 537.00 nm
Average RMS wavefront error (waves @ 527.50 nm): 0.386
Relative Field Throughput(%) Encircled_Energy(%) Spot50(um) Spot80(um)
0.000 65.68 91.36 4.446 7.436
0.350 65.68 91.91 4.408 8.205
0.500 65.68 91.24 6.861 12.763
0.707 65.50 87.92 4.697 7.443
0.850 65.14 85.50 2.732 5.609
1.000 64.24 68.81 3.215 5.602
+++++
Zoom position 5
Spectral bandpass center wavelength: 436.00 nm
Average RMS wavefront error (waves @ 423.10 nm): 1.064
Relative Field Throughput(%) Encircled_Energy(%) Spot50(um) Spot80(um)
0.000 65.68 67.43 3.215 5.602
0.350 65.68 72.52 4.476 7.761
0.500 65.68 70.22 5.110 8.248
0.707 65.50 61.07 7.584 12.200
0.850 65.14 57.20 8.017 12.585
1.000 64.24 39.97 6.397 11.687

```

**Figure 8** Performance summary of an improved throughput design. This design was optimized as a single configuration, operating over the spectral band from 0.4 microns to 1.0 microns.

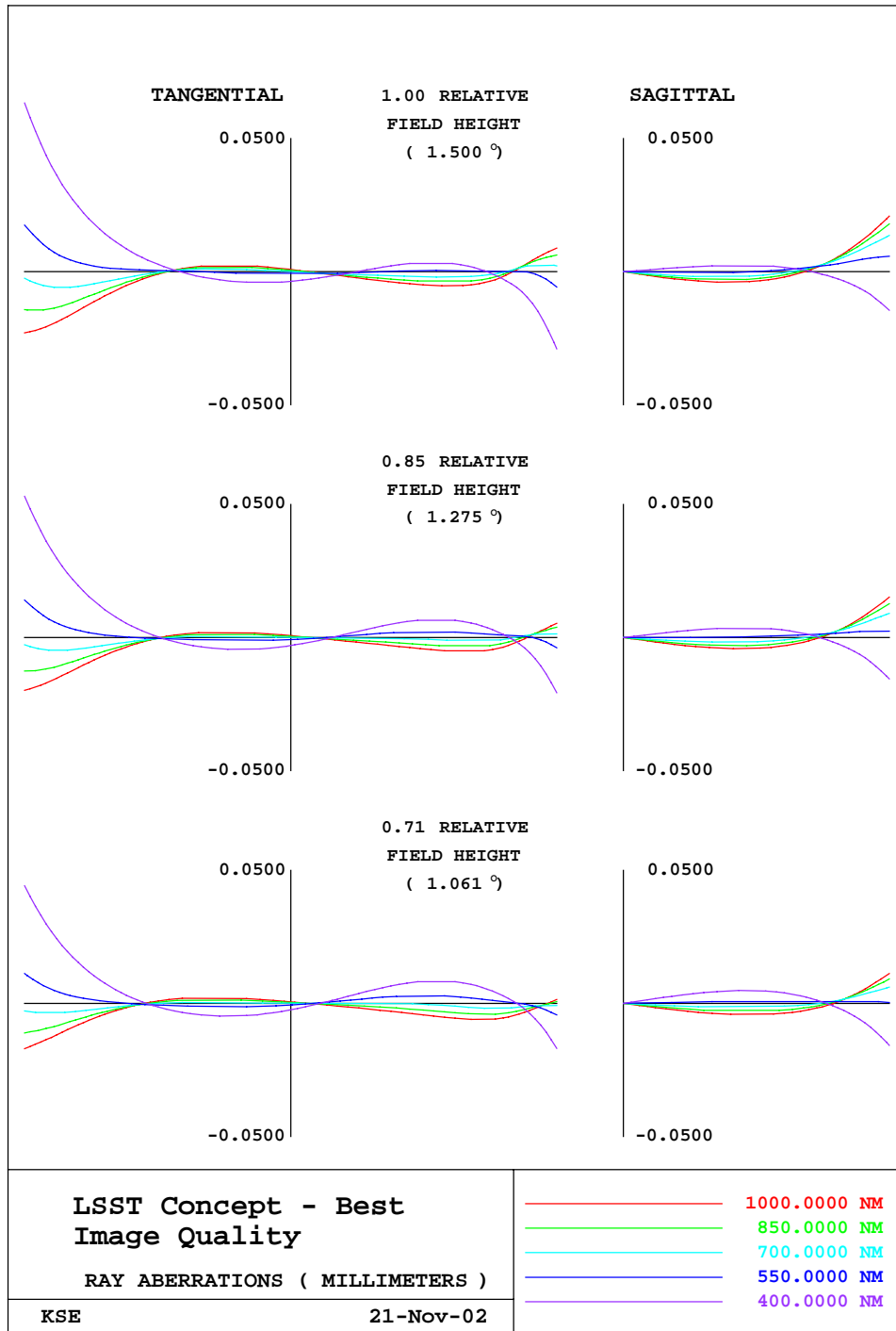


**Figure 9** Typical ray intercept plots (1.5, 1.275, and 1.06 degrees in descending order) for an optimized design.

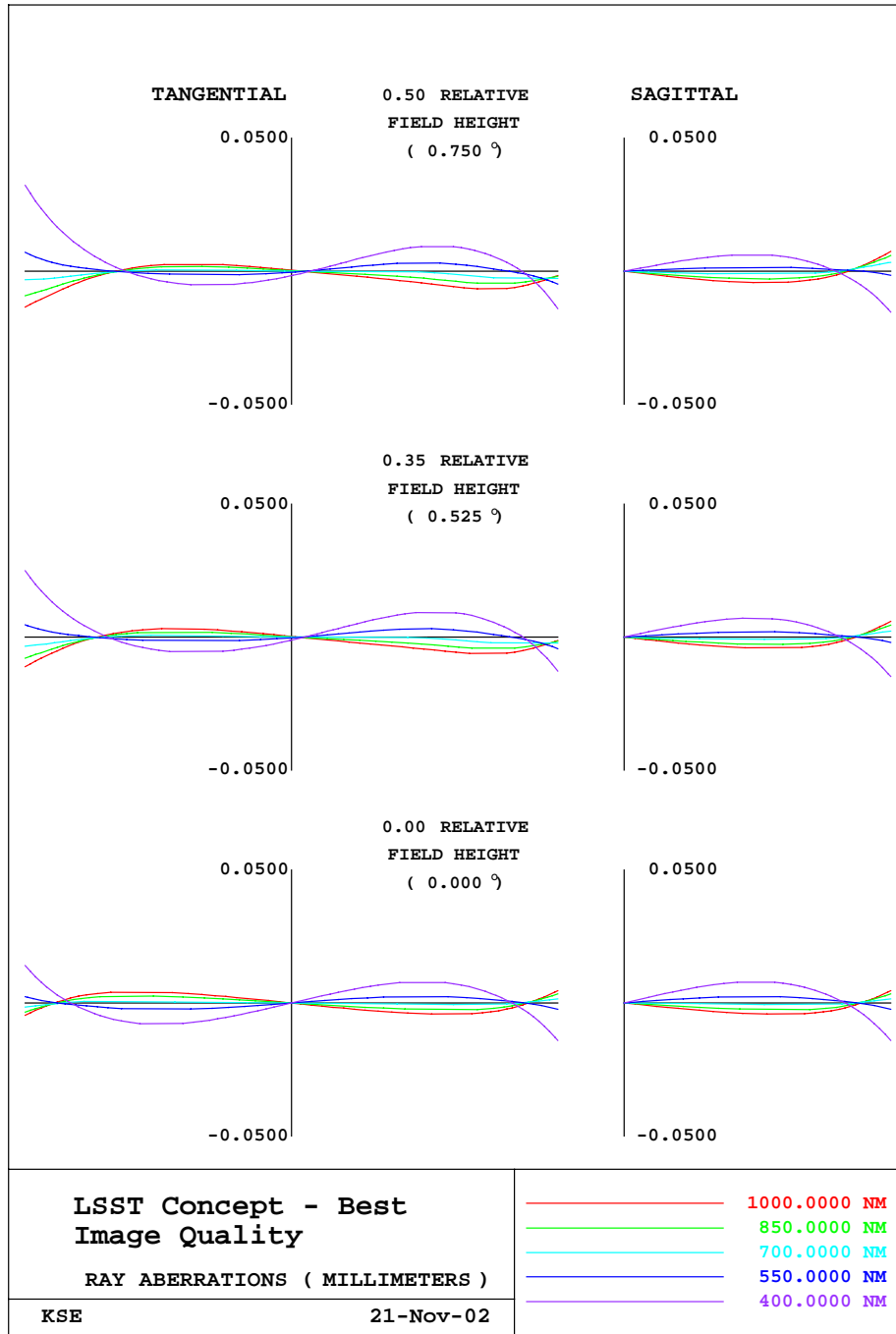


**Figure 10** Typical Ray intercept plots (0.75, 0.525, and 0 degrees in descending order) for an optimized design.

## Task 2 – Preliminary Baffle Design

Task 3 of the analysis includes the evaluation of baffle concepts and to identify possible baffle locations and their impact on fractional throughput. Of concern is the identification of specular illumination paths that reach the image surface. This task does not include either scatter or ghost image analyses. To complete this task, an optical system model was imported into FRED, Photon Engineering's commercially available optical engineering software (Figure 11). FRED is a generalized non-sequential raytrace analysis program that allows for the creation and analysis of optical and opto-mechanical system models.

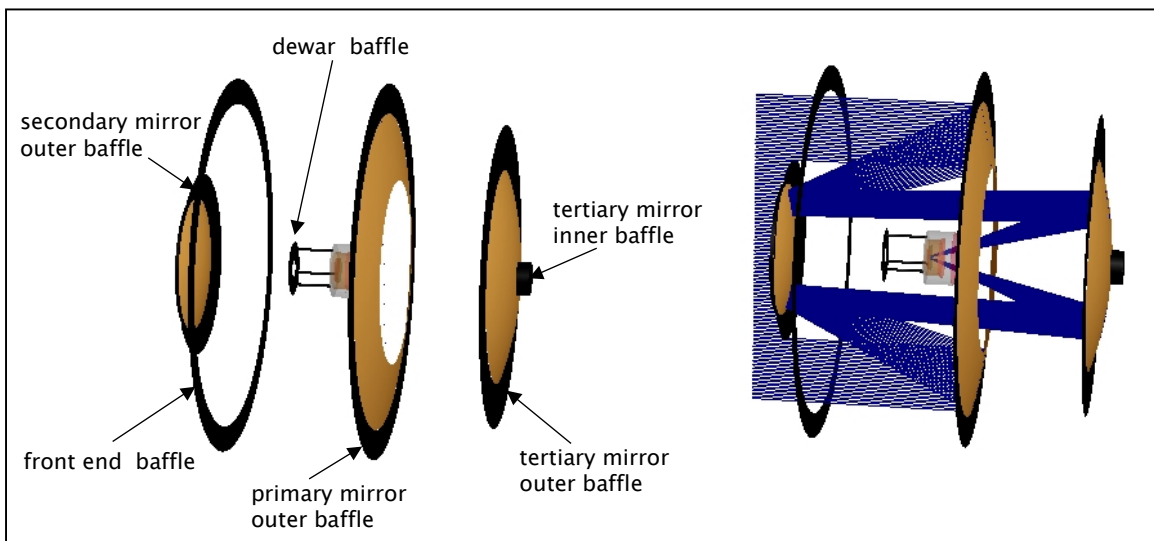


**Figure 11** FRED model of a baffled telescope showing suggested baffle configuration

The most efficient way to identify potential stray light paths is to launch rays from the detector surface backwards through the optical system. Doing so provides a first look at what the detector 'sees.' This technique identifies one potential specular path from outside of the field of view, shown in Figure 12 below. Figure 13 shows the raytrace of this path. Light incident on the telescope near an object space angle of 7.5 degrees strikes the primary and secondary mirrors in normal fashion. It then strikes the tertiary mirror, and, because the angle of incidence on the tertiary is nearly normal, is reflected back towards the secondary mirror. From the secondary mirror, light is reflected back again towards the tertiary mirror. The instrument assembly blocks most of the light on its return to the tertiary, but the remaining portion passes by and eventually reaches the detector along the normal imaging path. Although the net flux is quite low (~0.14%) and the image formed on the detector is diffuse, light traveling along this path would likely be detected by the instrument, resulting in measurement artifacts and erroneous data. Figure 14 shows the irradiance distribution arising from an extended source to give an indication

of the breadth of the problem. Point objects would not produce the same result, as they illuminate substantially less area.

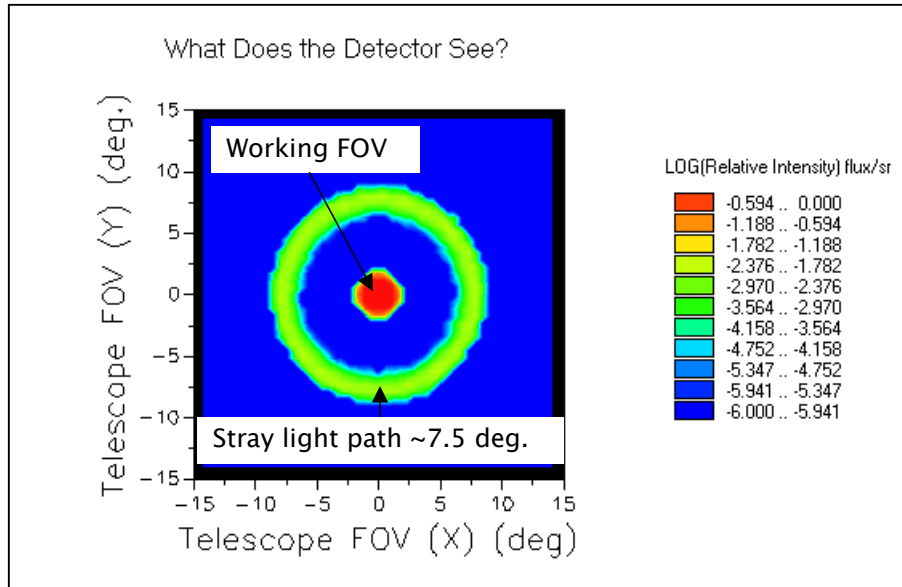


**Figure 12** Relative intensity plot (in object space) shows a significant stray light path occurring at ~7.5 degrees off-axis. Results were generated by tracing rays out from the detector

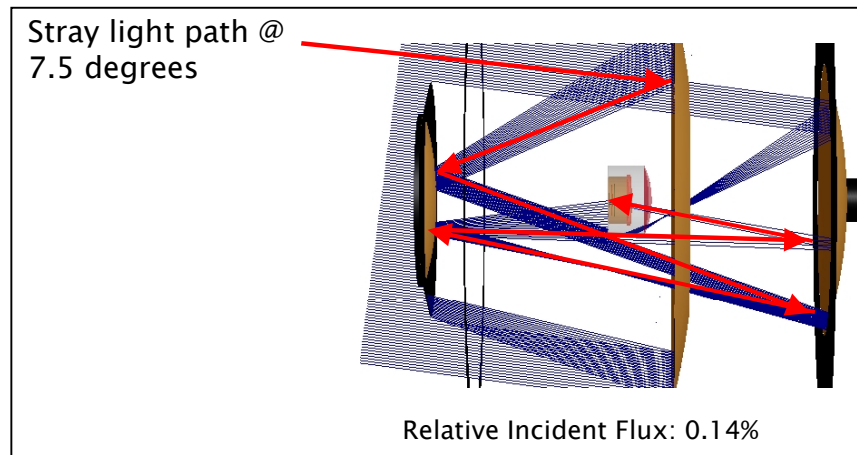


**Figure 13** Illustration of stray light path.

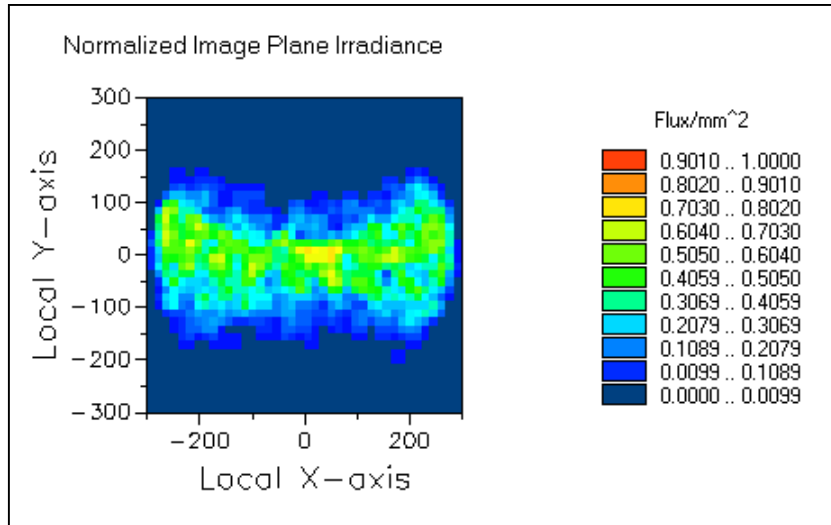


**Figure 14** Irradiance distribution on the image plane arising from an extended source tilted 7.5 degrees and emitting into a half angle cone of 1.5 degrees.

A single baffle located between the back side of the instrument assembly and the secondary mirror is all that is needed to suppress this path (Figure 15). It does not affect the fractional throughput because it is located in the shadow of the primary mirror obscuration. An alternative would be to place an annular baffle around the instrument assembly itself, but this baffle could potentially block light incident inside the field of view, thereby lowering throughput. Another advantage of moving the dewar baffle away from the instrument assembly is that it can be oversized slightly to block rays from striking the assembly at near grazing incidence, where most surfaces, even those painted black, exhibit high reflectivity.

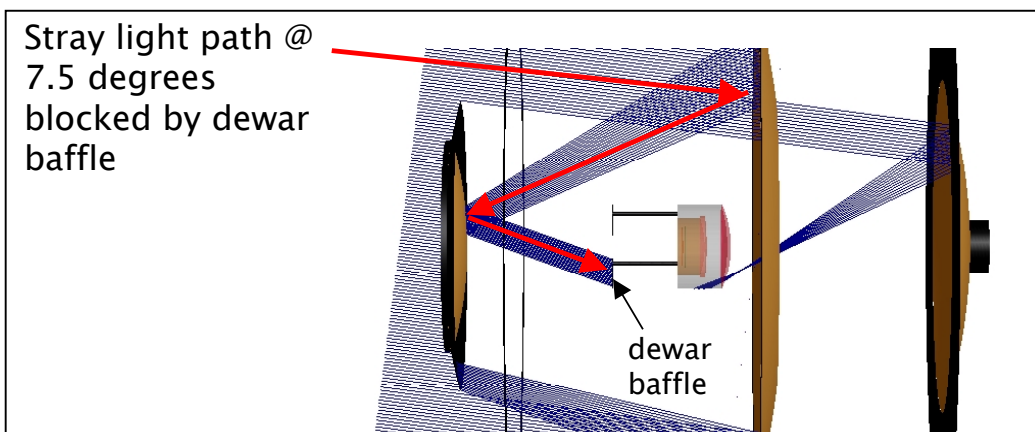


**Figure 15** Blocking effect of the dewar baffle.

Other paths exist which may not illuminate the detector directly, but can illuminate areas proximate to the detector active area, thereby increasing susceptibility to scattered light. One such path arises if the secondary mirror baffle (or obscuration if no baffle is used) is smaller than the hole in the primary mirror (Figure 16). Light that misses the secondary mirror and passes through the hole in the primary focuses inside the instrument ensemble. These rays are diverging quickly, but do manage to pass through Element 2. An on-axis source illuminates the inside wall of the inner dewar and perhaps even the active area if the secondary mirror obscuration is much smaller than the hole in the primary. Of more concern is light originating from a source located near the edge of the field of view because the rays that miss the primary and secondary mirrors can form an arc opposite the desired image inside the active area of the focal plane. This problem is again easily remedied by ensuring that the secondary mirror baffle is close to the same size as the hole in the primary.

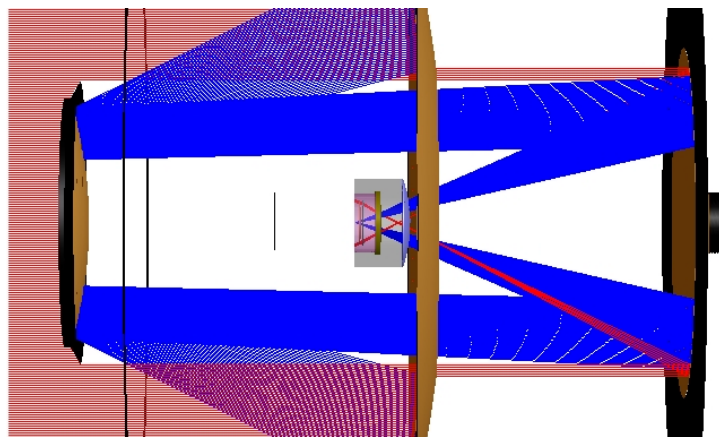


**Figure 16** Rays missing both the primary and secondary mirrors can reach the vicinity of the active detector area, a potential stray light risk.

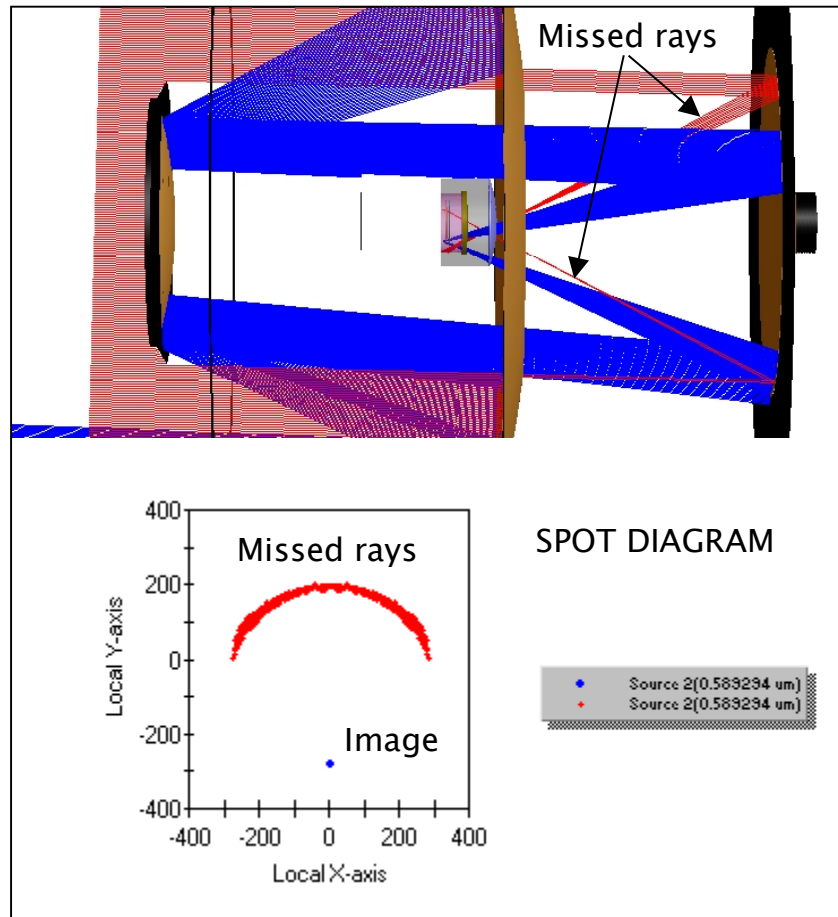


**Figure 17** Missed rays may illuminate the focal plane, as they do here, if the secondary mirror obscuration is too small.

### Task 3 - Fractional Throughput Analysis of Telescope with Baffles

A FRED model of the Case4b telescope was used to determine the effect of the baffles on the fractional throughput. Three configurations were evaluated. All of them use the apertures specifications suggested by Lynn Seppela in his SPIE presentation (ref. *SPIE\_4836-19\_10-01-02.pdf*) with the exception that the secondary mirror clear aperture diameter has been increased to 3690 mm, up from 3400 mm, to eliminate axial vignetting at the secondary mirror. The first configuration is a baffled telescope concept that uses the baffles proposed by Seppela and adds both a dewar baffle and a secondary mirror baffle cone. The latter has the same diameter as the hole in the primary. The raytrace for this model is executed non-sequentially. The second configuration removes all of the baffles and traces the rays sequentially through the optical system. This is analogous to the throughput calculations run in CODE V. The third configuration also removes the

baffles, but traces the rays non-sequentially to assess the relative contribution of rays that miss the primary and secondary mirrors, which turns out to be significant.

Fractional Throughput Calculations			
Semi-FOV (deg.)	With Baffles	No Baffles - Sequential	No Baffles - Non-sequential
0	0.70	0.70	0.74
0.525	0.70	0.70	0.73
0.75	0.69	0.70	0.74
1.061	0.68	0.68	0.72
1.5	0.62	0.63	0.66

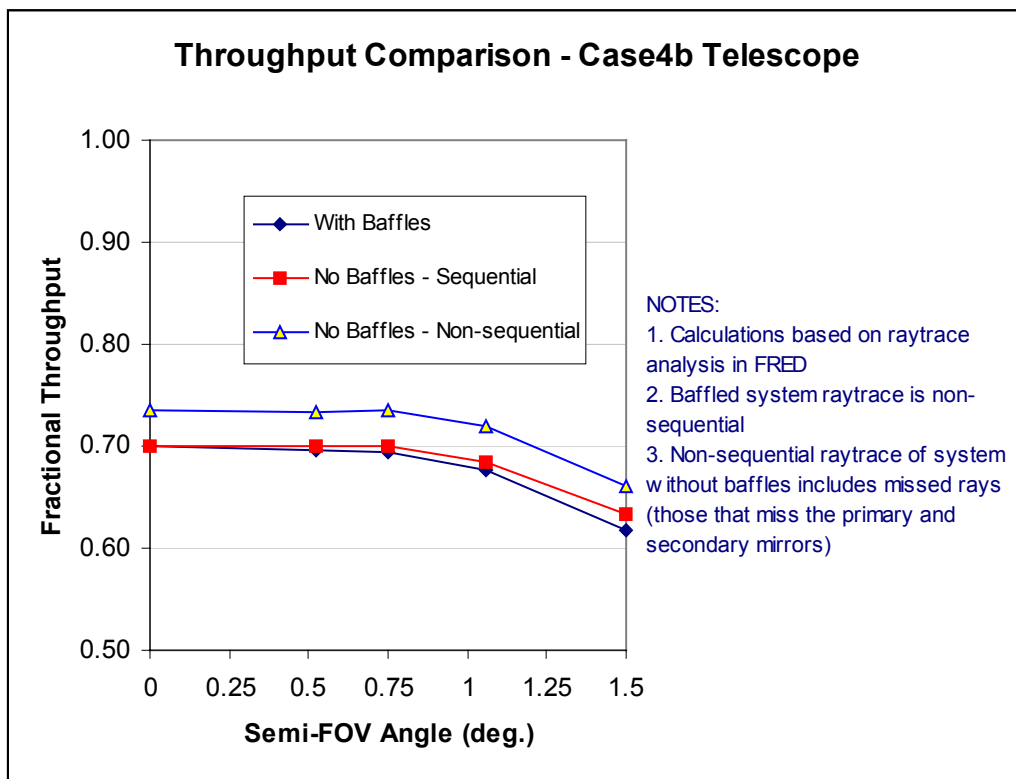


**Figure 18** Fractional throughput of the Case4b telescope under 3 raytrace conditions: a) baffled, non-sequential, b) no baffles, sequential, c) no baffles, non-sequential.

## Task 4 - Sensitivity Analysis

The position sensitivity of the primary, secondary, tertiary mirrors, and the instrument assembly was investigated. This was not a tolerance analysis. Instead, the goal was to identify how precisely the major telescope components must be held during the measurement cycle. The telescope is assumed perfect at the outset. Perturbations were applied singly to each component and were uncompensated. The perturbations on the mirrors were all rigid body motion about the vertex (real or virtual) of the individual surfaces. The instrument assembly was also subject to rigid body motion, with the origin being coincident with the front surface vertex of Element 1.

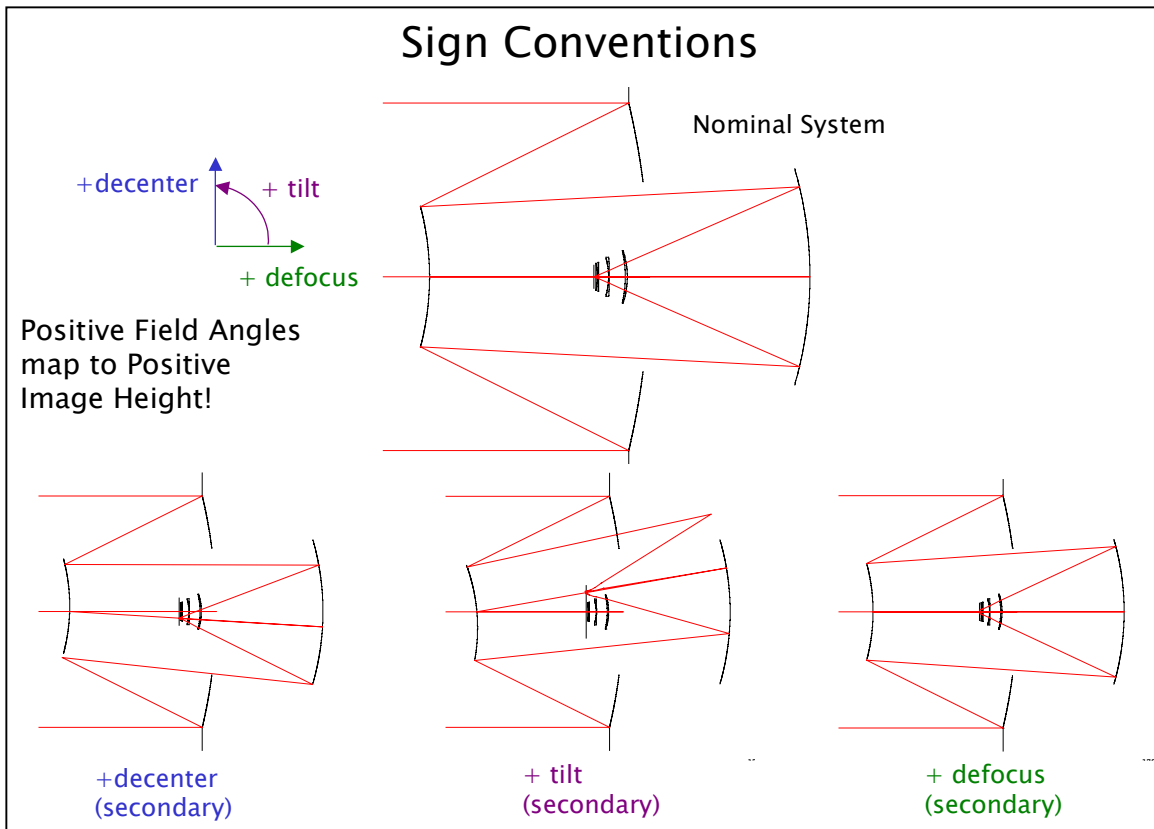
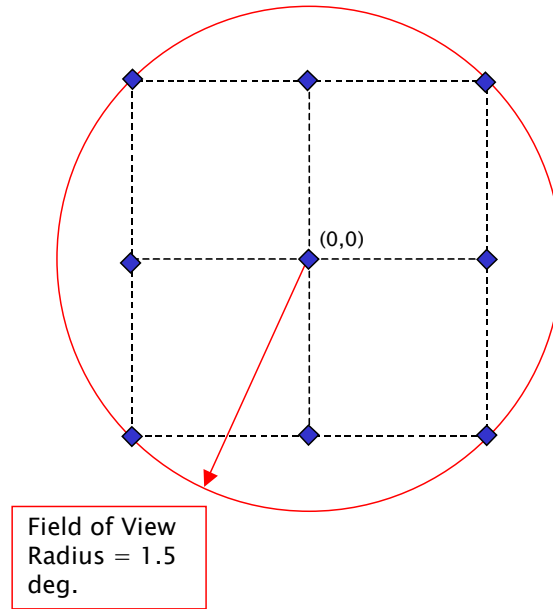


**Figure 19** Rigid body perturbations and sign conventions

The perturbations applied to each element were lateral decenter, axial decenter (defocus), and tilt about an axis perpendicular to the optical axis (Figure 19). Nine field points, distributed across the entire field of view, were used to assess image quality, boresight error (for tilt and decenter), and, for defocus, the resulting plate scale variation (Figure 20). Image quality was assessed as the growth in the blur diameter for both the 50% and 80% diffraction encircled energy spots. Boresight error is simply the change from zero of the on-axis ray intercept at the target plane divided by the focal length. Plate scale error was assessed as the change in the effective focal length of the telescope.

**Figure 20** Field point selection for sensitivity analysis



## Decenter Sensitivity

Spot size growth is assumed to be purely quadratic over the range of motion evaluated. The quadratic coefficients of each element and the range over which the approximation is valid is shown in Figure 21. The primary mirror is the most sensitive to centering errors.

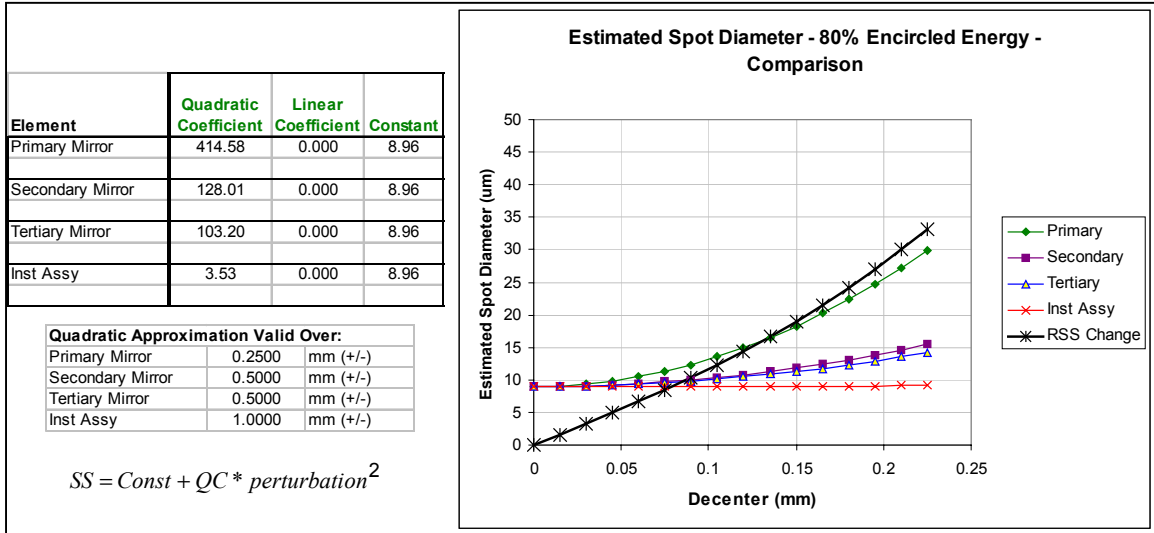


Figure 21 Element decenter (mm) and 80% diffraction encircled energy spot size degradation.

Angular boresight error is linear over the range of motion investigated, as seen in the following figure.

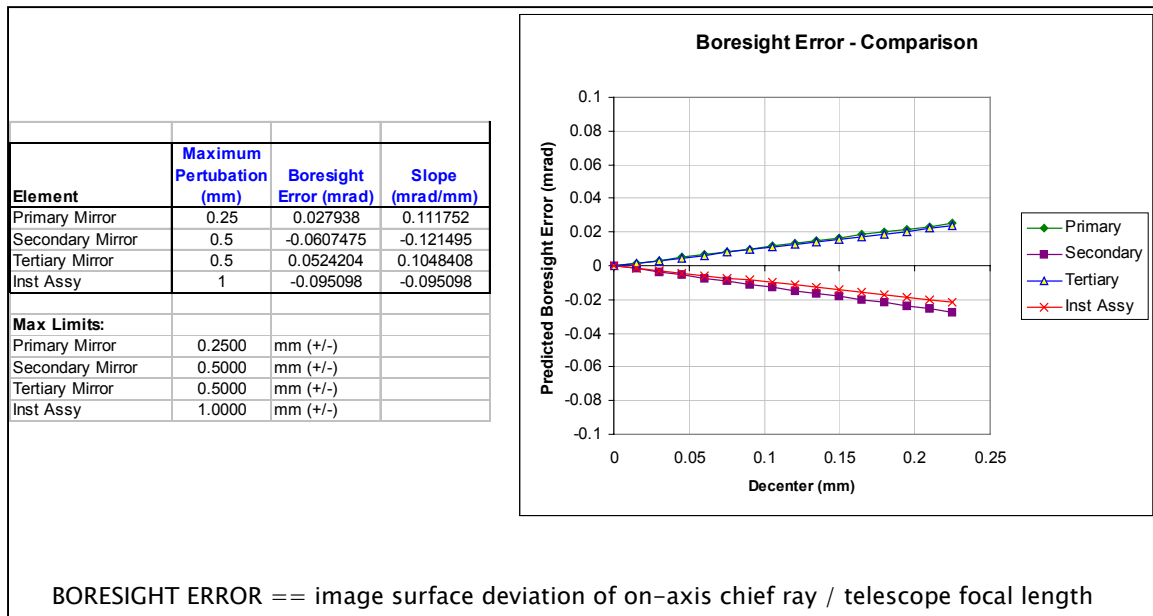
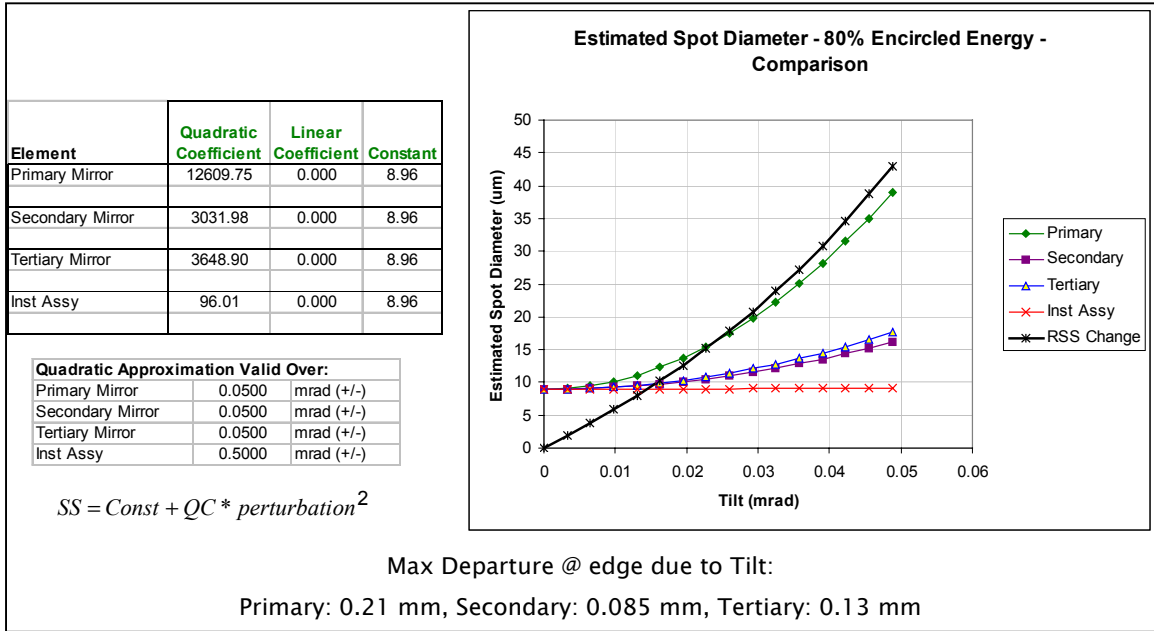


Figure 22 Angular boresight error resulting from centering errors

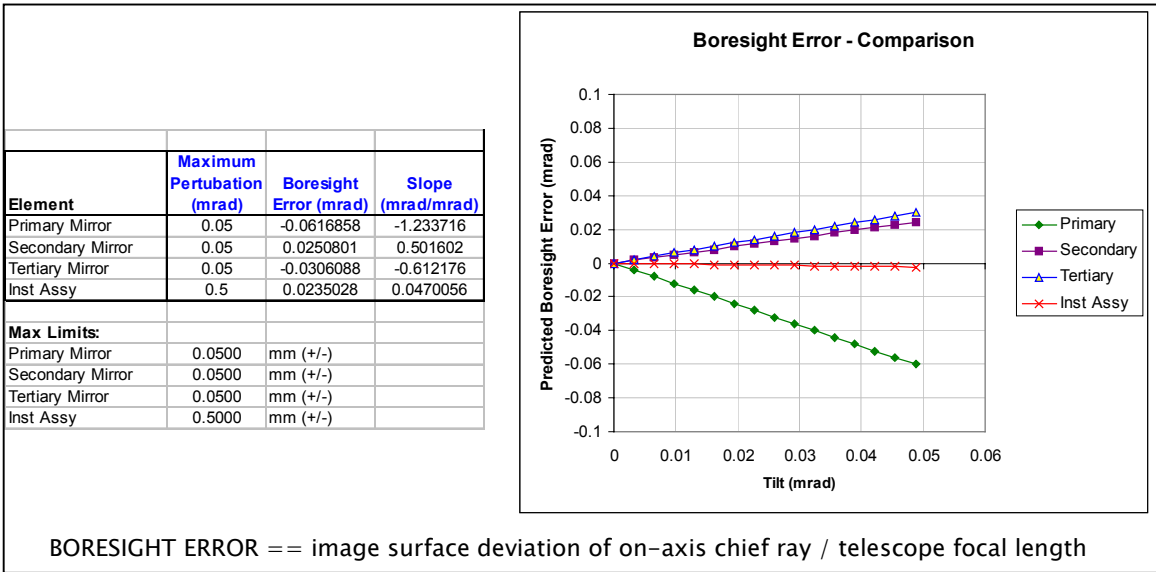
## Tilt Sensitivity

As was the case with decenter, the change in the encircled energy spot size grows quadratically with angle. Once again, the primary mirror has the highest sensitivity. Of note is that the tilt angles, while small, introduce a displacement error at the edge that is can be resolved using current sensing technology.



**Figure 23** Element tilt (mrads) sensitivity and 80% diffraction encircled energy spot size degradation.

Figure 24 shows boresight error resulting from element tilts. This error is linear, with the sensitivity coefficient being equal to the slope of the line.



BORESIGHT ERROR == image surface deviation of on-axis chief ray / telescope focal length

Figure 24 Angular boresight error resulting from element tilt errors

## Defocus Sensitivity

The sensitivity analysis for defocus showed that all major components contribute nearly equally to spot size growth and that the sensitivity coefficients are quite high, meaning that small perturbations lead to rapid change. It also shows that moving any one major component is as effective as any other for focus compensation.

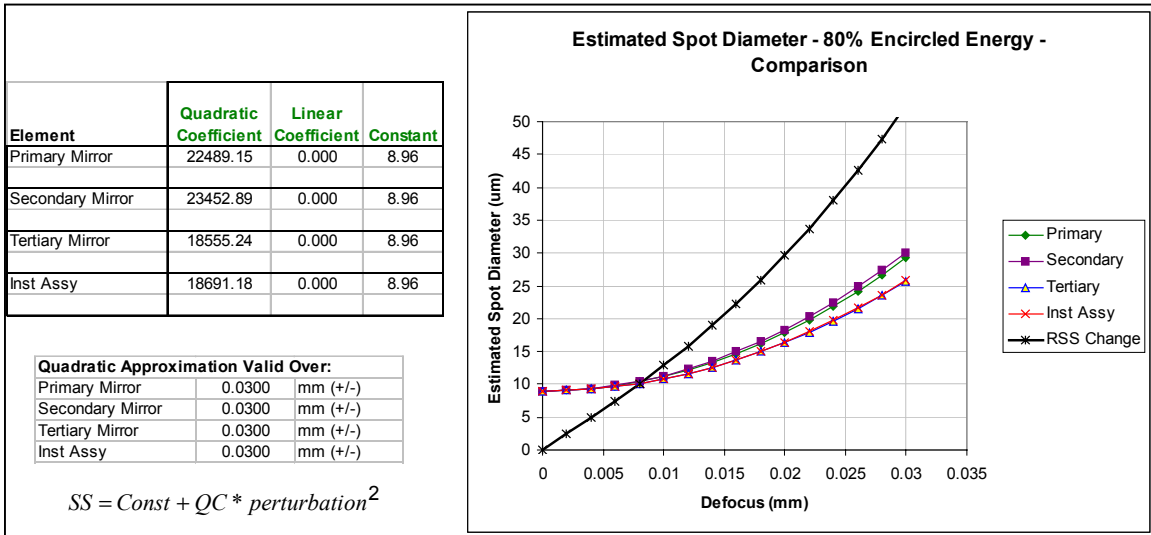


**Figure 25** Defocus (mm) sensitivity and 80% diffraction encircled energy spot size degradation.

Plate scale change was assessed by calculating the new paraxial focal length after each perturbation. Because the range of motion turns out to be quite small, the change in focal length is not significant, as shown in the following figure. Both the primary and secondary mirrors contribute in nearly equal magnitude, although the sign is different, indicating that motion in the same direction causes a reduction for one mirror and an increase for the other. For reference, a change in the focal length of 0.002% shifts the image 5.5 microns at the edge of the field of view. This calculation is based on the following relationship between focal length and paraxial object height.

$$\partial H = \left( 1 + \frac{\Delta\%}{100} \right) \cdot EFL_0 \cdot \tan(1.5)$$

The paraxial focal length of the telescope used in the calculation is 10500 mm.

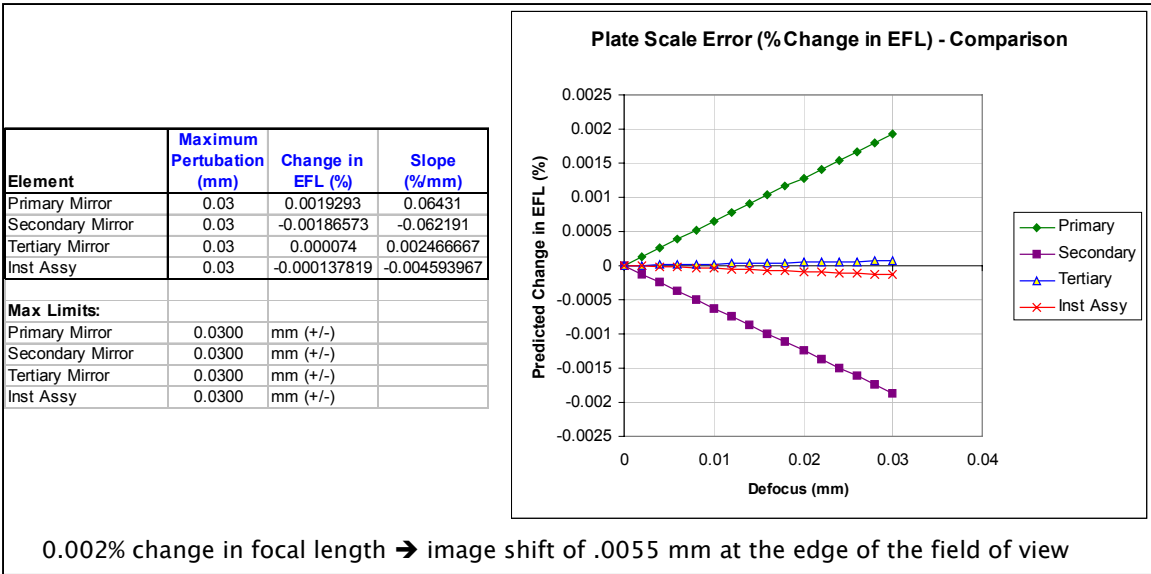


Figure 26 Plate scale variation as a function of element defocus.

## Concluding Remarks and Recommendations

This scope of this analysis was quite large, making it difficult for the reader to easily encapsulate the most important results, so they are summarized here.

The parametric analysis showed that there are a great many similar solutions that have similar levels of performance. Better throughput is obtained with a faster primary mirror, but these systems are not as well corrected. The hole in the primary mirror is the dominant mechanism for throughput loss. Sizing the hole to just pass the on-axis field yields the best throughput, but will result in significant variation across the field of view. Designing an unvignetted telescope can eliminate this variation, but the peak throughput falls shy of the 7m effective aperture specification.

Image quality for a single configuration broadband solution is not as good as that obtained with a multi-configuration design. The differences in some bands are substantial. Chromatic variation of the higher order aberrations, in particular spherical aberration and coma, is the limiting factor with regard to image quality. Changing materials did not prove to be an effective tool for correction. Adding another element also proved unsuccessful.

The addition of baffles, properly done, can eliminate direct illumination stray light paths without adversely affecting the fractional throughput of the system. The secondary mirror baffle should be about the same size as the hole in the primary mirror to keep rays that would otherwise miss both the primary and secondary mirrors from reaching the detector. An additional baffle between the instrument assembly and the secondary mirror is needed to block rays coming in at an angle of about 7.5 degrees to the optical axis. The baffle should be located in the shadow of the primary mirror obscuration so as not to affect the fractional throughput.

The sensitivity analysis showed that the primary mirror introduces error most quickly. Defocus sensitivity is quite high, with errors as small as 30 microns leading to substantial growth in the 80% encircled energy blur. It is believed that current technology can resolve and correct tilt and decentration.

## Reference Documents

The following documents have been submitted in conjunction with this report. Portions have been repeated here.

### Powerpoint files:

*Status1.ppt* – early progress on optimization and parametric analysis

*Throughput trades.ppt* – ongoing progress and summary of parametric analysis (optical design)

*Sensitivity analysis summary.ppt* – preliminary results of sensitivity analysis

*Case4b sensitivity analysis summary.ppt* – updated sensitivity analysis (includes diffraction encircled energy calculations)

### Excel files:

*Firstorder.xls* – spreadsheet to do quick first order layouts and estimate throughput of 3 mirror telescope configurations

*Sensitivity analysis 2.xls* – spreadsheet to tabulate and plot sensitivities based on degradation of encircled energy contained by a 10 micron diameter spot

*Case4b sensitivity analysis.xls* – added diffraction encircled energy calculation to *sensitivity analysis*.

*Case4b baffled system throughput analysis.xls* – data and chart showing throughput calculation results from FRED

### CODE V lens sequence files

*Lsst\_case4b\_zoom.seq* – original Case4b lens, zoomed for spectral bands

*Lsst\_case4b\_zoom\_global.seq* – original case4b lens, zoomed for spectral bands, element in global coordinate system to facilitate sensitivity analysis

*Lsst\_highest\_thru.seq* – 3 mirror configuration with f/1.05 primary mirror that demonstrates a good combination of throughput and image quality

*Lsst\_best\_imagequality.seq* – 3 mirror configuration based on a broadband solution of the Case4b design that satisfies Task 1 goals/constraints

### FRED files

*Lsst\_baffle\_designs.frd* – FRED model used to assess baffle concepts